Supporting Information for:

Crossover From Nanoscopic Intergranular Hopping to Conventional Charge Transport in Pyrite Thin Films

Xin Zhang, Michael Manno, Andrew Baruth, Melissa Johnson, Eray S. Aydil and Chris Leighton*

Department of Chemical Engineering and Materials Science, University of Minnesota, Minneapolis, Minnesota 55455, USA

***Corresponding author:** leighton@umn.edu.

I. Film Synthesis. FeS_2 films were fabricated using a two-step synthesis method. In the first step, 33 nm thick Fe films were deposited on $Al_2O_3(0001)$ substrates *via* D.C. magnetron sputtering from an Fe target (Kurt J. Lesker, 99.9 % purity). The primary impurities in the Fe target are O, Si, C, transition metals (Ni, Co, Cr, Cu), Ge, P and Al. The Ar pressure during deposition was 2.3 mTorr and the substrate temperature was 300 °C, resulting in a deposition rate of 0.08 nm/s and out-of-plane epitaxy with $Fe(011)//Al_2O_3(0001)$. In the second step, the Fe films were placed in evacuated (to 10^{-6} Torr) and sealed quartz tubes (8 cm^3) with 1.0 ± 0.1 mg of sulfur (CERAC, 99.999% purity), and sulfidized at temperatures from 100 to 800 °C (referred to as the sulfidation temperature, T_S). The sulfidation time-temperature trajectory comprised initial heating to T_S at 6.5 °C/min, followed by isothermal sulfidation at T_S for 8 h, then cooling at the natural cooling rate of the furnace. During a typical cooling period, the temperature decreases to 50 % of T_S within 4 h. The samples were positioned in the hottest location within the furnace to prevent sulfur condensation on the film surface during cooling. With 1.0 ± 0.1 mg of sulfur, solid or liquid coexists with vapor for T_S < 250 °C and the pressure in the tube is the sulfur vapor pressure [S1]. When T_S exceeds 250 °C all the sulfur is vaporized and the pressure in the tube approximately follows the ideal gas law. Using the published temperature dependence of sulfur speciation (*i.e.*, relative concentrations of S_x with $1 \leq x \leq 8$) in the vapor phase [S1], we estimate that the tube pressure ranged from 20 Torr at T_S = 250 °C to 45 Torr at T_S = 700 °C.

II. Structural Characterization. Wide angle X-ray diffraction (XRD) from FeS_2 films was collected using a Bruker-AXS Microdiffractometer equipped with a Cu source, a graphite monochromator (Kα pass-through filter), a 0.8 mm incident beam point collimator, and a 2D Hi-Star area detector. Two-dimensional XRD is ideally suited for small sample volumes such as thin

polycrystalline films because both specular and non-specular diffracted x-ray intensities in a wide range of 2θ values are collected simultaneously. This allows for longer dwell times at each diffraction angle and increases the signal-to-noise ratio.

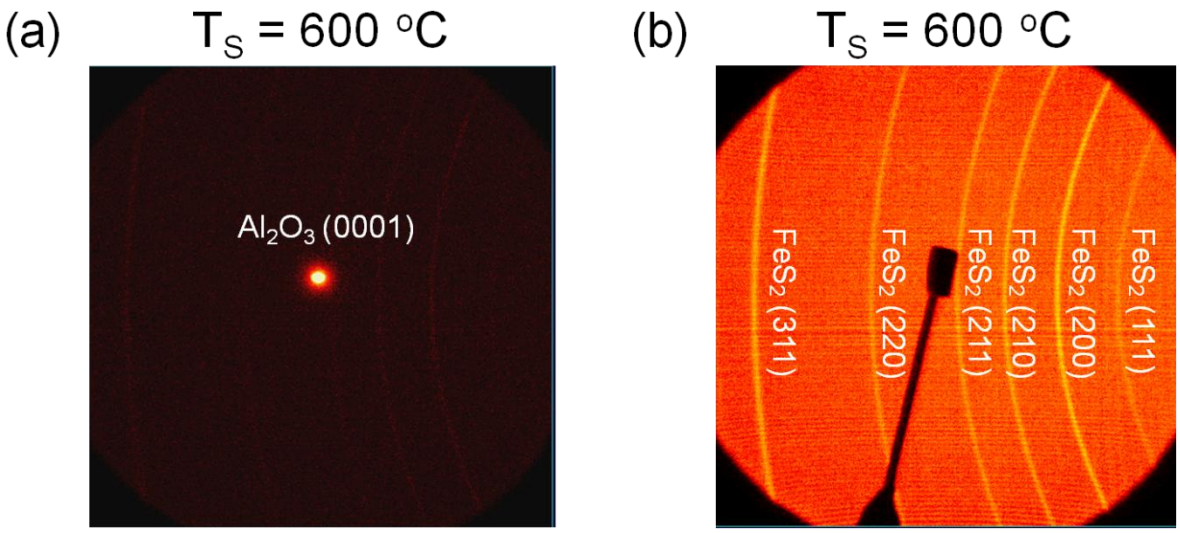

Figure S1. WAXRD two dimensional detector images for a 33 nm thick Fe film sulfidized at 600 °C. (a) An image acquired using a short exposure time (1 min) and including the Al_2O_3(0006) diffraction from the substrate. (b) An image acquired using a longer exposure time (30 min) after blocking the Al_2O_3(0006) diffraction from the substrate with a beam stop. In (b) the Debye rings are labeled with the pyrite FeS_2 (*hkl*).

The following XRD data collection protocol was adopted for quantitative comparison of diffraction intensities from films sulfidized at different T_S. First, the substrate coated with the film was aligned to maximize the Al_2O_3(0006) diffraction peak intensity. Following this, consecutive XRD patterns were acquired for one and thirty minutes, respectively. During the thirty-minute-long acquisition, a beam stop was used to block the Al_2O_3(0006) diffraction peak. Figures S1(a) and (b) display example area-detector images from the first (one minute long) and

second (thirty minute long) XRD acquisitions, respectively, for a film sulfidized at T_S = 600 °C. Two-dimensional XRD data such as those shown in Figure S1 were integrated and converted to one-dimensional intensity *vs.* 2θ plots. For quantitative comparison, the second (thirty minute acquisition) XRD pattern was normalized by the film thickness and the Al_2O_3(0006) diffraction peak intensity recorded during the first scan (one minute acquisition). These normalized patterns were used to generate the XRD data shown in Figures 1 and 3 of the manuscript. The Al_2O_3 substrate reflection was used as a standard for more accurate determination of the FeS_2 lattice parameter.

The microstructure and chemical composition of the films were examined using a JEOL field emission scanning electron microscope (SEM) equipped with a Thermo-Noran Vantage energy dispersive spectrometer (EDS). Both plan view and tilted view (85° tilted angle) SEM images were acquired using an accelerating voltage of 15 kV.

A Physical Electronics model 545 Auger electron spectrometer (AES) with a differentially-pumped Ar sputter source was used to map composition as a function of depth (z). We define z = 0 as the FeS_2/Al_2O_3 interface. The location of this interface was determined from the onset of the charging effects that occur in the insulating Al_2O_3 substrate. Values of z were assigned assuming a constant sputtering rate, found to be 7.65 nm/min from thickness measurements by tilted SEM. Figures S2(a) through S2(c) display elemental depth profiles of FeS_2 films sulfidized at T_S = 200 °C, 400 °C and 600 °C, respectively. The Fe:S ratio is seen to be quite uniform throughout the film. In order to plot absolute atomic compositions, these AES data have been calibrated against EDS. Due to the cratering effect, the FeS_2/Al_2O_3 interface is instrumentally broadened to ≈20 nm.

The interface region (grey shading) exceeds this instrumental width at T_S = 600 °C only, indicating measurable substrate/film interdiffusion at these higher T_S. The very small Al and O signals through the entire depth of the film are simply attributed to noise, although their importance at the semiconductor dopant level cannot be ruled out.

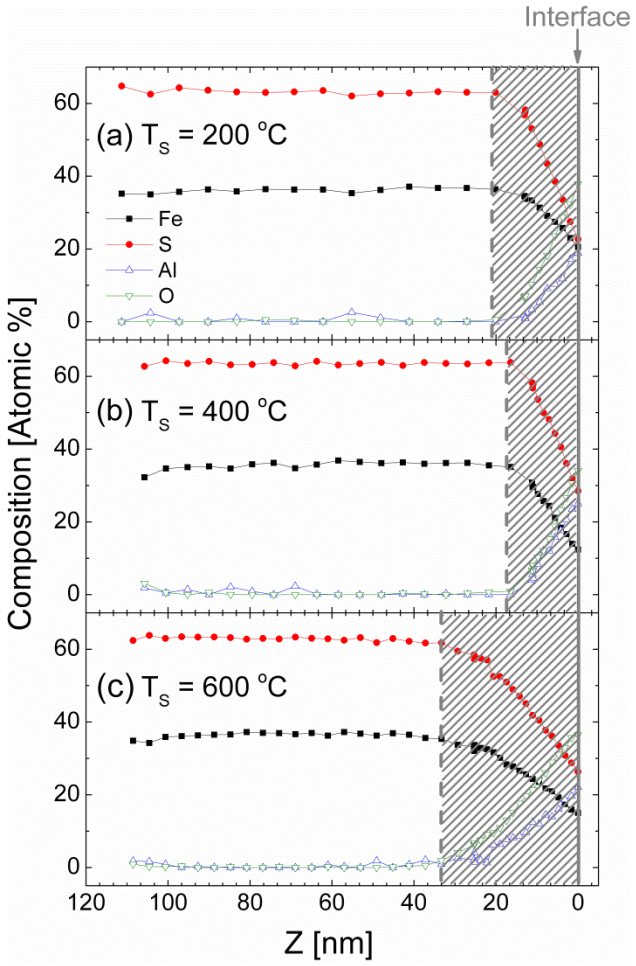

Figure S2. Elemental composition (Fe, S, Al and O) as a function of depth (z) in FeS_2 films sulfidized at (a) 200, (b) 400, and (c) 600 °C. The films were approximately 110 nm-thick. The Al_2O_3/FeS_2 interface is labeled and defined as z = 0. The shaded areas indicate the interfacial region.

Raman scattering from FeS_2 films was collected in the backscattering geometry using a WiTec alpha300R confocal microscope equipped with a UHTS 300 spectrometer and a DV401 CCD detector. Figures S3(a) through S3(c) display examples of Raman spectra from FeS_2 films sulfidized at T_S = 200 °C, 400 °C, and 600 °C, respectively. Strong Raman scattering peaks at 343, 380 and 430 cm^{-1} indicate the presence of the FeS_2 pyrite phase [S2], while the lack of spectral peaks at 315 – 324 cm^{-1} and ≈ 385 cm^{-1} indicate the absence of the marcasite phase [S2].

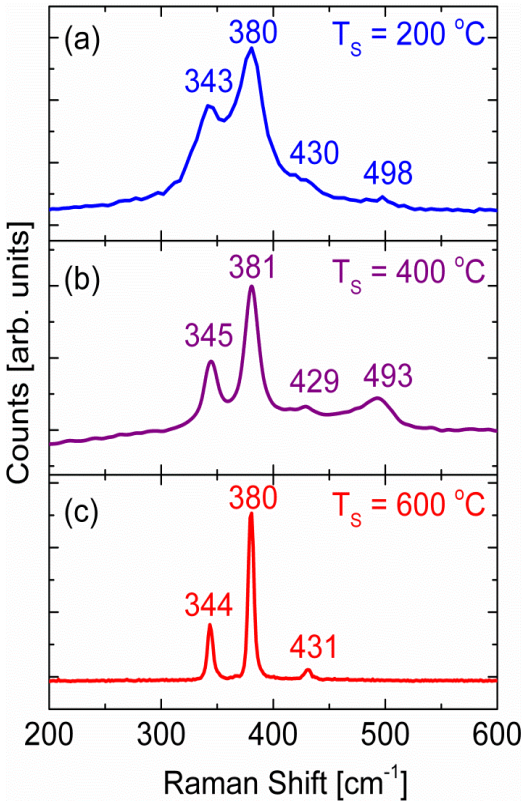

Figure S3. Raman spectra of 110 nm-thick FeS_2 films sulfidized at (a) 200, (b) 400, and (c) 600 °C. The peaks around 343, 380, and 430 cm^{-1} are assigned to pyrite FeS_2 based on prior work [S2]. The peak near 490 - 500 cm^{-1} may be associated with residual S [S1]. No marcasite FeS_2 (expected peak positions of 315 – 324 cm^{-1} and ≈ 385 cm^{-1}) was detected.

III. Transport Measurements. Temperature- and field-dependent measurements of resistivity and Hall effect in FeS_2 films were made in a Janis He flow cryostat equipped with a 9 T (90 kOe) superconducting magnet, between measuring temperatures of 5 and 300 K. Hall measurements employed a measurement system optimized for low noise AC measurements (using an AC resistance bridge) and high temperature stability. The latter is particularly important for films such as these with high temperature coefficient of resistance. The FeS_2 films were contacted with indium in a van der Pauw configuration, and current-voltage characteristics were measured using both A.C. (at 13.7 Hz) and D.C. techniques, depending on the absolute resistance value. As mentioned in the methods section of the manuscript, extensive checks for Ohmicity, contact resistance, and self-heating were made. At low temperatures a positive magnetoresistance signal necessitated the use of standard symmetrization techniques (see ref. S5 for instance) to separate the Hall signal from the magnetoresistance.

To complement the data shown in the manuscript, Figures S4(a) and S4(b) show a ln ρ *vs.* T^{-1} plot for FeS_2 films sulfidized at $T_S \leq 550$ °C and a ln ρ *vs.* $T^{-1/2}$ plot for $T_S \geq 500$ °C, respectively. The lack of adherence to T^{-1} behavior for $T_S \leq 550$ °C, and the lack of adherence to $T^{-1/2}$ for $T_S \geq 500$ °C is apparent. Note in particular the distinct upward curvature at $T_S = 600$ °C in Figure S4(b), indicating that the T dependence is distinctly stronger than $T^{-1/2}$ as $T \rightarrow 0$. To complement Figure 4(d) of the main manuscript, in Figure S4(c) we plot ln W *vs.* ln T over the entire measurement temperature range. The crossover from a slope of ½ to a slope near 1 in the low T limit is clear, as is a crossover to a weaker high T dependence for the highest T_S values.

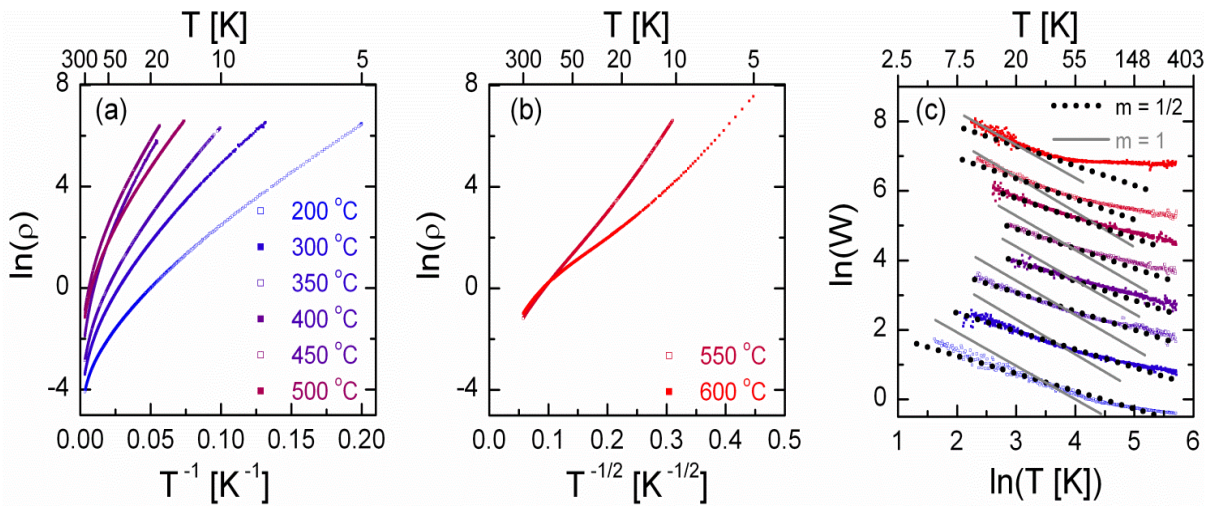

Figure S4. Additional data on the temperature dependence of the resistivity: (a) shows ln ρ *vs.* T^{-1} for films sulfidized at temperatures 500 °C and below; (b) shows ln ρ *vs.* $T^{-1/2}$ for films sulfidized at temperatures 550 °C and above; (c) shows ln W *vs.* ln T, for all samples, over the entire measurement temperature range. In (c), lines with slopes of m = ½ and 1 are also shown for comparison, where m is the exponent in $\rho = \rho_0 \exp (T_0/T)^{-m}$.

Magnetoresistance (MR), defined as $[\rho(H) - \rho(0)] / \rho(0)$, is the relative change in resistivity due to an applied magnetic field, H. Figures S5(a) and S5(b) show MR as a function of out of plane H (to 90 kOe), at various measuring temperatures, for films sulfidized at T_S = 200 °C and 400 °C, respectively. The T dependence of the MR at 90 kOe is plotted in Figure S5(c) for the same films. While the sign of the MR at 90 kOe is positive for the FeS_2 sulfidized at T_S = 400 °C, its dependence on T is inconsistent with Efros-Shklovskii Variable Range Hopping (ES VRH) [S3]. In particular, the MR saturates at 1.5 % at 15 K (Figure S5(c)), in sharp contrast to the expected divergence as $T \rightarrow 0$. This discrepancy with ES VRH theory is even more acute at T_S = 200 °C,

where the MR is non-monotonic with *H* and *T*, even changing sign below 10 K. It is likely that these anomalous effects originate from intergranular hopping between magnetic grain cores.

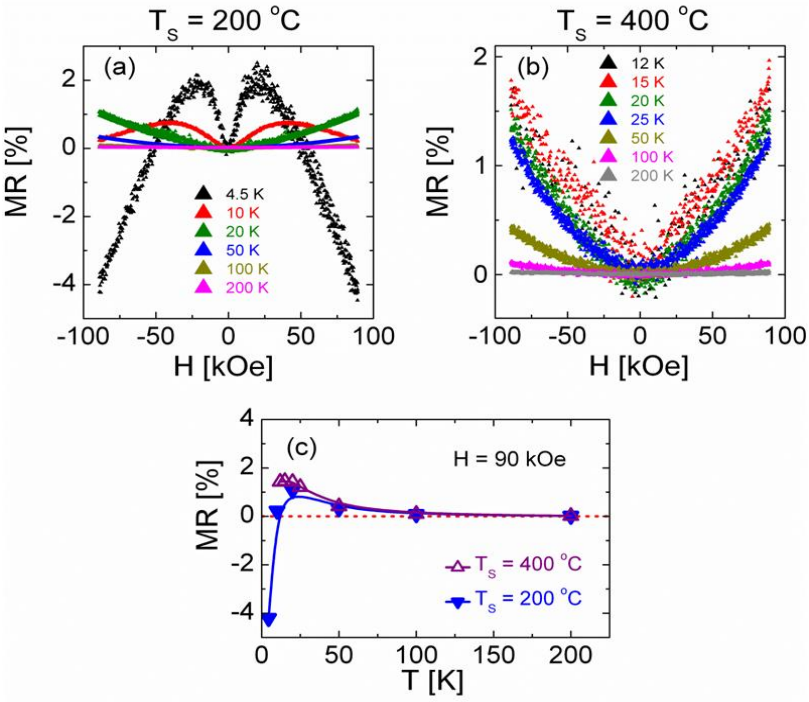

Figure S5. Magnetoresistance (MR) of 110 nm-thick FeS_2 films sulfidized at 200 and 400 °C. (a) and (b) show the field dependence of MR at multiple temperatures, whereas (c) shows the temperature dependence of the MR at 90 kOe. Solid lines are guides to the eye.

IV. Hall Effect Measurements. Figure S6 displays the *H* dependence of the Hall resistivity (ρ_{xy}) between ±90 kOe at a measuring temperature of 290 K for FeS_2 films sulfidized at 200 °C, 400 °C, and 600 °C. The ρ_{xy} data for the FeS_2 film sulfidized at T_S = 200 °C have been multiplied by 100 for clarity, and the zero field Hall resistivity has been subtracted from all curves. As expected the Hall resistivity is linear in *H*. Note the change in sign between 200 and 400 °C, from hole-like to electron-like, which is discussed in detail in the manuscript.

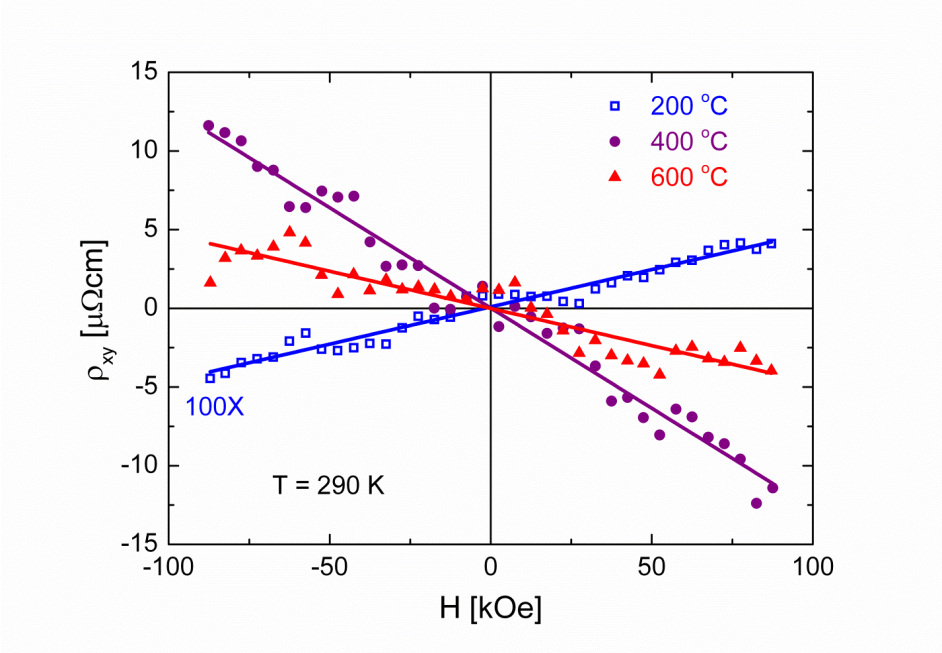

Figure S6. Magnetic field dependence of the Hall resistivity (ρ_{xy}) at 290 K for 110 nm-thick FeS_2 films sulfidized at 200, 400 and 600 °C. The values for the film sulfidized at 200 °C have been multiplied by 100. The solid lines are straight line fits.

Measurements of the type shown in Figure S6 were also made as a function of temperature. Figure S7 shows an example data set for a film synthesized at T_S = 400 °C, plotting the temperature dependence of the Hall carrier density (n_{Hall}), the resistivity (ρ), and the resulting Hall mobility (μ). The carrier density is observed to freeze-out by two orders of magnitude on cooling from 300 to 25 K, while the mobility exhibits only a weak decrease. This decrease in mobility with cooling indicates that the mobility is not yet limited by phonon scattering, broadly consistent with the room temperature value of approximately 0.1 $cm^2V^{-1}s^{-1}$, which indicates that such films lie in the crossover region between hopping and diffusive transport.

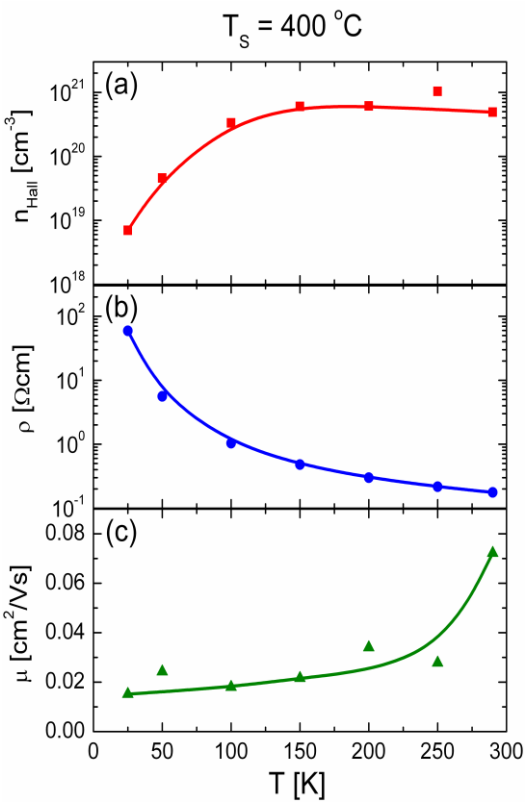

Figure S7. Temperature dependence of the carrier density (n_{Hall}, (a)), the resisitivity (ρ, (b)) and the carrier mobility (μ, (c)) for a 110 nm-thick FeS_2 film sulfidized at 400 °C. Solid lines are guides to the eye.

V. Magnetometry Measurements and Associated Analysis. Magnetometry measurements were conducted in a superconducting quantum interference device (SQUID) magnetometer from 5 to 300 K in fields up to 7 T (70 kOe). We provide in this section more details on the analysis of the data provided in Figs. 6(a) and (b) in the manuscript. As shown in Fig. 6(a), at T_S = 200 °C we obtain a saturation magnetization of 0.04 μ_B/Fe. Assuming that this magnetization arises from the presence of unsulfidized metallic Fe at the center of the FeS_2 grains, the average volume of these Fe cores can be calculated from the measured magnetic moment and the known saturation

magnetization of Fe [S4]. The resulting volume fraction of Fe was calculated to be as little as 0.5 vol. %, which is below our WAXRD detection limit, which we estimate to lie at at least 5 vol %. Taking this unreacted Fe volume to be spherical in shape and to lie at the center of the FeS_2 grains, the diameter of the Fe core is given by $d_{core} = (0.005)^{1/3}\, d_{grain} = 10$ nm, where d_{grain} is the measured FeS_2 grain size. The blocking temperature (T_B) for a superparamagnetic particle can be related to its volume through the equation $T_B = (K_u V/k_B)\ln(\tau f_o)$ [S4], where K_u (5.2×10^5 erg/cm^3) is the anisotropy constant of Fe [S4], τ is the time scale relevant for the measurement, and f_o is the attempt frequency, typically 10^9 Hz. For our measurements $\tau \approx 100$ sec. Using this expression, with no adjustable parameters, T_B is then predicted to be 72 K, which agrees very well with the measured value (78 K). As discussed in the manuscript this agreement is not at all satisfactory when other Fe-S compounds are assumed to be retained at the grain core. As an example, if we were to assume that the grain cores were comprised primarily of pyrrhotite, a lower S content compound for which the magnetic properties are also well-known [S6], we would require a volume fraction of 20 %, well above our XRD detection limits. This is therefore inconsistent with our observations. Moreover, the blocking temperature calculation in this case yields an extremely high temperature, indicating that the magnetic moment would remain thermally stable to the Curie point (around 580 K), again clearly inconsistent with our measurements. As discussed in the manuscript, the situation is similar for other potential Fe-S phases.

References

S1. Meyer, B. Elemental Sulfur. *Chem. Rev.* **1976**, *76*, 367–388.

S2. Berry, N.; Cheng, M.; Perkins, C. L.; Limpinsel, M.; Hemminger, J. C.; Law, M. Atmospheric-Pressure Chemical Vapor Deposition of Iron Pyrite Thin Films. *Adv. Energy Mater.* **2012**, *2*, 1124–1135.

S3. Shklovskii, B. I.; Efros, A. L. *Electronic Properties of Doped Semiconductors*; Springer series in solid-state sciences; Springer-Verlag: Berlin; New York, 1984.

S4. O'Handley, R. C. *Modern Magnetic Materials: Principles and Applications*. Wiley, 2000.

S5. Wang, S.; Ha, M.; Manno, M.; Frisbie, C. D.; Leighton, C. Hopping Transport and the Hall Effect Near the Insulator–Metal Transition in Electrochemically Gated Poly(3-Hexylthiophene) Transistors. *Nat. Commun.* **2012**, *3*, 1210–7.

S6. Dekkers, M. J. Magnetic Properties of Natural Pyrrhotite Part I: Behaviour of Initial Susceptibility and Saturation-Magnetization-Related Rock-Magnetic Parameters in a Grain-Size Dependent Framework. *Phys. Earth Planet. Inter.* **1988**, *52*, 376–393.